AIAA 80-1319R

Laser Ignition of Plasma Off Aluminum Surfaces

G. Weyl,* A. Pirri,† and R. Root‡
Physical Sciences, Inc., Woburn, Mass.

The prompt initiation of a plasma above metal surfaces irradiated by a CO_2 laser pulse in an intensity range of $10^6 - 10^9$ W/cm^2 is modeled. The initiation mechanism is assumed to be the vaporization of flakes or surface defects that are thermally insulated from the bulk surface, followed by laser-induced breakdown in the vapor. The fluid dynamics of the expansion in an air background is modeled in one- and three-dimensional regimes. Breakdown of the vapor due to inverse bremsstrahlung absorption of the laser radiation is calculated specifically for aluminum by use of a Boltzmann code. Results are presented in the form of a map of breakdown time vs incident laser flux and compared with available experimental data.

Nomenclature

A = area
a = α_I/α_I
B = 1.5×10^{-13} W$^{-1}\cdot$cm^{2}K, Eq. (22)
$b(x)$ = shape function for excitation cross-section
C_p = specific heat
c = speed of light
c_s = speed of sound
e = electron charge
f_{ij} = oscillator strength for transition $i \rightarrow j$
g = statistical weight
g = $n_{e0}/(2an)$, Eq. (36)
$H_{m,v}$ = heat of melting, vaporization
h = Planck's constant
I = intensity
$I_{\text{INC, ABS, REF}}$ = incident, absorbed, and reflected intensity
i = intensity normalized to 10^6 W/cm^2
k = thermal diffusivity
k_B = Boltzmann constant
m = mass
$\dot{m}$ = mass flow rate
M = Mach number
n = density
n_{e0} = initial electron density, Eq. (34)
p = pressure
r = radial position, radius
R = radius of flake (= 6 μm)
T = temperature
t = time
t_c = characteristic time in breakdown model, Eq. (39)
u = velocity
x = coordinate
α = absorption coefficient
α_I, α_I = rate coefficient for excitation, ionization
β = coefficient in Clausius-Clapeyron relation
γ = ratio of specific heats (= 5/3)
δ = flake thickness (= 0.2 μm)
ϵ = energy
θ = angle of incidence
θ_v, θ_I = vaporization and ionization energies, K
ν = collision frequency
ω = laser angular frequency, 1.77×10^{14} s^{-1}
ω_p = electron plasma frequency
ρ = mass density
σ = cross section
σ_{ij} = cross section for excitation of state j from state i
τ_v = time to start vaporizing
τ_{VBr} = time to breakdown
τ_{3D} = time for three-dimensional effects
χ = absorption coefficient, Eq. (29)
$\bar{\chi}$ = $\chi/(n_e n)$

Subscripts

A = of atom
e = of electrons
i, j = of states i, j (i = 1-4)
I = for ionization
m = momentum transfer
s = at surface
sh = at shock
v = for vaporization
0 = ground state
1 = first excited state
5 = in region 5, Fig. 1
∞ = ambient conditions

Superscripts

$(^*)$ = at sonic conditons
$(\tilde{\ })$ = normalized to conditons at 10^6W/cm^2
$(+)$ = for ion
$\langle\rangle$ = average value of

Received March 14, 1980; presented as Paper 80-1319 at the AIAA 15th Fluid and Plasma Dynamics Conference, Snowmass, Colo., July 14-16, 1980; revision received Sept. 3, 1980.

*Principal Scientist.
†Manager, Laser Applications. Member AIAA.
‡Principal Scientist. Member AIAA.

I. Introduction

THE prompt initiation of a plasma above metallic surfaces irradiated with CO_2 laser fluxes of 10^6-10^9W/cm^2 is not completely understood. These plasmas in an air environment grow rapidly, developing into either a laser-supported detonation (LSD) wave[1] or a laser-supported combustion wave[2] which absorbs the laser radiation and strongly influences the laser coupling to the surface. It is important to understand the plasma initiation mechanisms in order to control the laser coupling to the surface by promoting or suppressing plasma ignition. Musal[3] has made the empirical observation that the gain-switched spike of a CO_2 laser pulse will cause prompt ignition if the spike fluence is greater than 1 J/cm^2 and if the spike intensity is above 10^7W/cm^2.

Previous studies[4-6] of prompt ignition have considered many phenomena which may provide the initial electron concentration. There exists, however, to the authors' knowledge, no comprehensive theory which adequately treats both the problem of initial electron population and the growth of this population to the point of gas breakdown. The initial

electrons can be provided by field emission from protrusions,[4] thermionic emission,[5] equilibrium ionization in the hot vapor,[5] and shock heating of the air by the rapidly expanding vapor.[6] Through detailed experimental studies, Walters et al.[7,8] indicate that the initiation mechanism is very probably associated with presence of surface defects such as flakes which are thermally uncoupled from the bulk material. They showed that before a flake vaporizes it could create, by thermionic emission, an electron sheath of the order of the Debye length with an electron density in the range 10^{13}-10^{15}cm^{-3}. They then calculated the time to breakdown in air by assuming that these electrons gain energy through inverse bremsstrahlung absorption of the laser beam, *all* of the energy being converted into ionization of the gas, thereby providing a mechanism for cascade breakdown of the air. They were thus able to explain the breakdown data in the flux range 10^{7}-10^{8}W/cm^2. Breakdown times in the shock-heated air in front of the vapor piston have been calculated in a similar fashion by Steverding.[6] It has, however, been well established experimentally[9] and theoretically[10,11] by detailed solutions of the electron kinetic equation that cascade ionization in air does not occur at fluxes below 10^{9}W/cm^2: attachment to oxygen (as well as excitation of rotational, vibrational, and electronic states) provides a sink for all the electron energy. Edwards et al.[12] used the sophisticated two-dimensional LASNEX code to study initiation of LSD waves off an aluminum surface. In order to obtain prompt vaporization (in the absence of surface defects which they did not consider), they postulated that the thermal conductivity of aluminum decreased by a factor of 10 above the melting temperature. Their treatment of the breakdown was also unphysical since they neglected inelastic collisions other than ionization collisions between the electrons and the air molecules. Thomas and Musal[5] studied the one-dimensional vaporization of an aluminum surface. They followed the breakdown assuming a two-temperature model for the vapor, with one exicted state for aluminum. The excited state formed an energy sink for most of the electron energy. Cascade ionization occurred through electon impact ionization of the ground state of aluminum by electrons having an energy larger than 6 eV. Nielsen[13] treated the breakdown of a cesium vapor by solving the kinetic equation and showed that a two-temperature model, such as that used by Musal, will yield breakdown times that are too short by a factor of three at a flux of 10^{7}W/cm^2, the discrepancy getting larger as the intensity is reduced below this value. Nielsen, however, did not couple his vapor breakdown calculations with the dynamics of vapor formation and expansion.

We present here a model of plasma initiation which relies on the vaporization of a thermally insulated flake. The formation of vapor before breakdown has been well established experimentally by Reilly,[14] who measured resonant absorption in aluminum (and other metal vapors for varying metal targets) along a path grazing the surface. Initial electrons are provided by thermal ionization in the vapor. When the flake starts vaporizing, the expansion of the vapor drives a shock in the air and we follow the laser-induced breakdown in the vapor during the expansion process. If the breakdown is sufficiently rapid (this will occur at fluxes $I>3\times10^{7}\text{W/cm}^2$ for Al at 10.6 μm), the expansion can be treated as one-dimensional, the gas density remains high, and collisional processes are rapid. If breakdown has not occurred by the time a fluid element has traveled a distance away from the surface comparable to the flake radius, then three-dimensional effects become important and the vapor overexpands to supersonic velocity; a recompression wave will move in toward the surface and result in the formation of a stationary shock, which brings the vapor pressure back to near atmospheric. Breakdown is then expected to occur in the vapor behind the shock. The geometry for the one- and three-dimensional expansion cases is shown in Fig. 1. The breakdown time τ_{vBr} is found to increase significantly as one goes from the one-dimensional geometry (at high intensity) to the three-dimensional geometry (at low intensity). Finally, at a sufficiently low laser intensity, where the vapor that comes off the surface is at a pressure below atmospheric, mixing of vapor with air dominates and breakdown is not expected to occur (at least during the laser pulse for pulse lengths of interest). The plasma initiation time is the sum of τ_v and τ_{vBr}, and we will show that at high fluxes τ_{vBr} is so small that τ_v dominates. At low fluxes the main delay is due to τ_{vBr}.

Vaporization of a flake and expansion of the vapor are treated in Sec. II. Breakdown in the vapor phase is analyzed in Sec. III with specific results for aluminum. We have used a Boltzmann code which treats the effects of electron-electron collisions, excitation of several lower lying electronic states of aluminum, and ionization from the ground state and excited states. An important input to the code is the initial electron density. This density is calculated by assuming a Saha equilibrium of the vapor just as it leaves the surface. We have also derived in Sec. III analytic results for the breakdown process which are useful for scaling breakdown times with laser intensity and wavelength. The results of this study are presented in Sec. IV in the form of a map of breakdown time vs laser flux, and a comparison of our results with limited experimental data is made. Conclusions are presented in Sec. V.

II. Flake Heating and Vaporization

We investigate in this section the rapid heating of surface defects or flakes and the subsequent expansion of the vapor once the surface of the flake has reached the vaporization temperature. A flake is thermally uncoupled from the bulk metal. If the flake thickness δ is much smaller than the thermal diffusion thickness $(k\tau_p)^{1/2}$ (k = heat diffusivity, τ_p = pulse time), then heating of the flake can be taken as

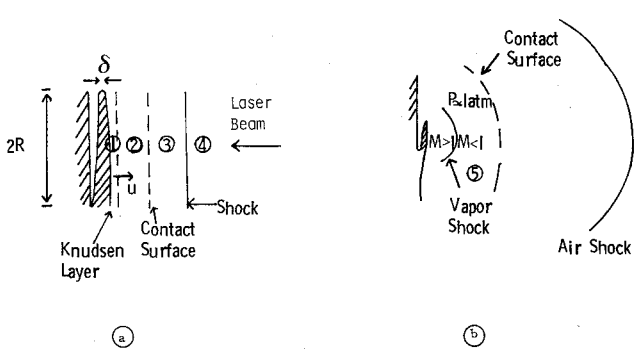

Fig. 1 Geometry for vapor breakdown: a) one-dimensional expansion, b) three-dimensional expansion; regions 1, 2, and 5 correspond to metal vapor. Breakdown is expected to occur first in region 2 (one-dimensional) or 5 (three-dimensional).

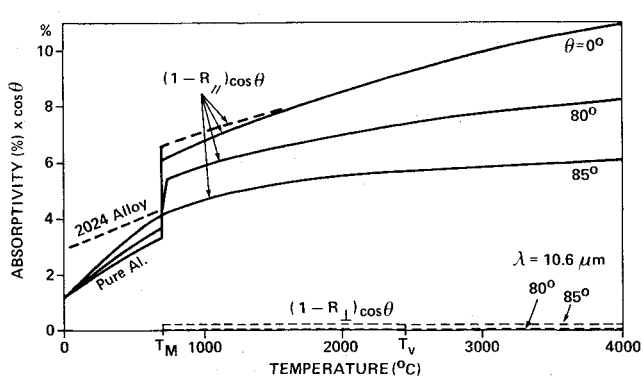

Fig. 2 Absorptivity of aluminum vs temperature for several angles of incidence θ [subscripts $\parallel$ ($\perp$) refer to electric field in (out of) plane of incidence].

Table 1 Properties of Aluminum

Condensed Phase		Pure aluminum	Al 2024 alloy
Density ρ,	g/cm^3	2.7	2.7
Specific heat C_p,	J/g	0.90	0.92
Heat conductivity K,	W/cm K(T = 300 K)	2.37	1.89
Heat diffusivity k,	cm^2/s	0.98	0.76
Melting temperature T_m,	°C	660	660
Vaporization temperature T_v,	°C	2467	2467
Absorptivity α,	%(λ = 10.6 μm, T = 300 K)	1.2	3
Absorptivity α,	%(λ = 10.6 μm, 3000 K)	10 (est.)	10 (est.)
$[\langle 1/\alpha \rangle]^{-1}$	%(300 - 3000 K)	4	5

	State j						
Vapor phase	0	1	2	3	4	5	ion
ϵ_j, eV	0.0	3.142	3.605	4.02	4.085	4.67	6.0
g_j	6	2	12	10	6	2	1

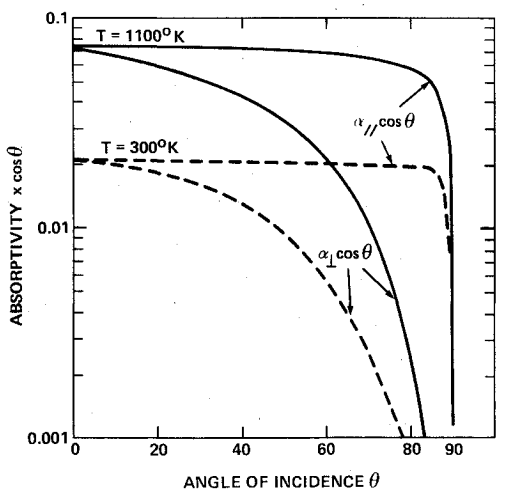

Fig. 3 (Absorptivity × cos θ) vs angle of incidence θ (aluminum, $\lambda = 10.6$ μm).

uniform during the pulse. The time τ_v for the flake to reach a temperature T_v, where vaporization becomes important, is given by the solution of

$$\int_0^{\tau_v} I_{\mathrm{INC}}(t)\,\mathrm{d}t = \int_{T_0}^{T_v} \frac{\rho C_p \delta}{\alpha \cos\theta}\,\mathrm{d}T \tag{1}$$

where I_{INC} is the laser intensity incident on the surface, α the surface absorptivity, and θ the angle of incidence. The relevant properties for aluminum, as found in standard handbooks, are given in Table 1.

The absorptivity α is expected to be a strong function of T. Available absorptivity data for aluminum are to be found only for the metal near room temperature. In order to calculate its absorptivity over the range 300-3000 K, we have used the Drude theory for metallic reflection,[15] together with measured values of room temperature reflectivity,[16,17] and measured values[18] of resistivity of pure aluminum vs T in the range 0-1200°C. The approach is based on the fact that only two parameters are required to specify the dielectric function of a metal, namely, the electron plasma frequency ω_p (or equivalently effective number density of free electrons) and the collision frequency ν of electrons with the lattice.[19] Analysis of the reflectivity data yields these two quantities at room temperature and the variation of resistivity with temperature yields the variation of one of them (ν), the other (ω_p) having been assumed to remain constant. Figure 2 shows the calculated absorptivity for three angles of incidence at 10.6 μm. The sharp rise in absorptivity at 660°C is due to melting of the material. The absorptivity is seen to rise from a very low value (~1%) at room temperature to almost 10% at the vaporization temperature. We show in Fig. 2 the effects of angle of incidence on the absorption coefficient. One sees from Fig 3 that the absorbed intensity, $I_{\mathrm{INC}}\alpha\cos\theta$, for parallel polarized radiation (electric field in the plane of incidence) is independent of angle of incidence up to very large angles. This is to be compared with the absorbed intensity for perpendicular polarization which drops drastically as θ increases. An approximation for $\alpha_{||}$, which is valid to order $\omega^2/(\omega_p^2\cos^2\theta)$ (ω is the laser angular frequency), is given by

$$\alpha_{||} = \frac{4\omega}{\omega_p}\frac{(1+\nu^2/\omega^2)^{1/2}}{\cos\theta}\sin\left(\frac{1}{2}\tan^{-1}\frac{\nu}{\omega}\right) \tag{2}$$

From the data of Ref. 17, at room temperature $\nu = 1.7 \times 10^{14}\,\mathrm{s}^{-1}$ and $\omega_p = 1.5 \times 10^{16}$. The average of $1/\alpha$ from room temperature to 2500°C is found to be 20, i.e., we can use $\langle\alpha\rangle = 5\%$ in Eq. (1) to describe the heating process up to the vaporization temperature.

We will consider in the following the case of normal incidence, the results obtained being the same for oblique incidence and parallel polarization. For large angles of incidence and an unpolarized beam, the absorbed fluence will be lower by a factor of two than that used in this paper. If the beam has a constant intensity I_{INC}, the time to reach vaporization temperature can be calculated explicitly by integration of Eq. (1).

$$\tau_v = \frac{\delta[\rho C_p(T_v - T_0) + H_m]}{\langle\alpha\rangle I_{\mathrm{INC}}} = \frac{10\delta(\mu\mathrm{m})}{I_{\mathrm{INC}}(\mathrm{W/cm^2})} \tag{3}$$

where H_m (= 400 J/g) is the latent heat of melting of the metal (Al). Equation (3) tells us, for example, that for $I_{\mathrm{INC}} = 10^7\,\mathrm{W/cm^2}$ and $\delta = 0.2$ μm we will have $\tau_v = 200$ ns which is orders of magnitude smaller than if we had considered vaporization with the inclusion of heat conduction through the bulk metal where $\tau_v = [(T_v - T_0)\rho C_p/\alpha I_{\mathrm{INC}}]^2 k \cong 150$ μs. Equation (3) will be useful even for laser intensities that are not constant in time. In this case I_{INC} will represent an average intensity over the time required to vaporize the flake.

Once the vaporization temperature has been reached, vapor is blown off the surface of the flake with a mass rate per unit area given by $\dot{m} = \alpha I_{\mathrm{INC}}/H_v$, with $\alpha \cong 0.1$ and with a heat of vaporization $H_v \cong 10^4\,\mathrm{J/g}$ ($= 7.8 \times 10^{-12}\,\mathrm{erg/atom}$) for aluminum. The expansion of the vapor at early time drives a planar shock in the air as shown schematically in Fig. 1a, and the expansion can be considered as one-dimensional. We study below the vapor properties for the one-dimensional expansion and then consider the three-dimensional later time vapor expansion.

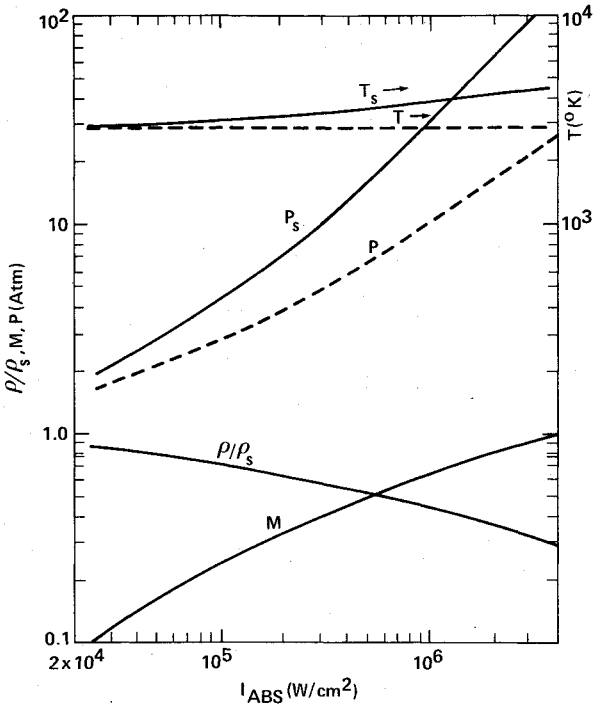

Fig. 4 Vaporization of aluminum in air (P_s, T_s, and ρ_s refer to properties at surface; P, ρ, and T to properties in region 2 of Fig. 1a; M is Mach number in region 2).

One-Dimensional Expansion

Analysis of one-dimensional expansion of vapor into a vacuum has been performed by Anisimov[20] and into air by Thomas,[21] Pirri,[22] and Knight.[23] We use in this paper the results of Knight. The geometry is shown in Fig. 1a. Very near the surface in region 1 there is a Knudsen layer which extends over a few mean free paths. In this layer the one-sided Boltzmann distribution of metal atoms emanating from the surface at temperature T_s and pressure p_s is converted into a spherically symmetric distribution with p and T. Region 2 is a region of uniform vapor properties with pressure p and temperature T. Region 3 is the region of shocked air and region 4 is the undisturbed atmosphere ahead of the shock where the pressure is p_∞ and the temperature T_∞. Assuming that p_s and T_s are related through the Clausius-Clapeyron relation for saturated vapor and that the sticking coefficient for particles impacting on the surface is unity, Knight was able to calculate the vapor properties in regions 1 and 2 as a function of absorbed flux $I_{ABS}=\alpha I_{INC}$. The results for aluminum for $p_\infty=1$ atm are plotted in Fig. 4.§ The flow in region 2 is subsonic when $I_{ABS}\lesssim 3.8\times10^6$ W/cm^2 ($I_{INC}\lesssim 3.8\times10^7$ W/cm^2). It is interesting to note that the pressure at the surface p_s scales almost linearly with flux and that the temperature in region 2 is practically constant ($T\cong 3000$ K) over the whole intensity range considered. Extrapolating the results to lower fluxes, we find that when $I_{ABS}<10^4$ W/cm^2 $p_s<1$ atm so that the vapor diffuses into the air.

Analytic approximations (good to within 5%) to the curves plotted in Fig. 4 for $I_{ABS}>2\times10^5$ W/cm^2 will be useful in scaling vapor breakdown times. They are the following:

$$\tilde{p}_s = i^{1.10} \tag{4}$$

$$\tilde{T}_s = i^{0.084} \tag{5}$$

$$\tilde{n}_s = i^{1.01} \tag{6}$$

$$(\tilde{\rho/\rho_s}) = i^{-0.23} \tag{7}$$

The $\sim$ sign refers to quantities normalized to those pertaining to $I_{ABS}=10^6$ W/cm^2 and i is the absorbed flux in MW/cm^2. The reference vapor properties at an absorbed flux of 10^6 W/cm^2 are given in Table 2.

Vapor Expansion in Three Dimensions

The length scale for three-dimensional effects is the transverse radius R of the flake. The transverse dimension of the flake is estimated from electron micrograph studies of the surface to be in the 1-10 μm range.[8] The one-dimensional model presented in the previous subsection is strictly valid only for times such that the air shock is within one radius of the surface. We can define the time for three-dimensional effects to become important as the time it takes the vapor to travel a distance R away from the surface. Let the velocity of the vapor be u. We have

$$\tau_{3D}=\frac{R}{u}=\frac{R}{Mc_s}\cong 8\times10^{-10}\frac{R(\mu\text{m})}{M} \tag{8}$$

where c_s is the sound speed and M the Mach number. We used the fact that $T\cong 3000$ K in the last step of Eq. (8). If we make $R=6$ μm and set $M=0.4$ ($I_{ABS}=3\times10^5$ W/cm^2) we calculate $\tau_{3D}=10^{-8}$ s. If the breakdown has not occurred by the time the shock has traveled a distance R, the initially planar shock will become spherical and the vapor-air contact surface will also become spherical. The vapor will overexpand. An expansion wave will move in toward the flake, accelerating the flow in the vapor until the flow chokes at the surface. The edge of the Knudsen layer then becomes sonic and vapor conditions are as given by Anisimov.[20] A shock will form in the vapor, which at late times occupies a stationary position with respect to the surface. The purpose of the shock is to raise the vapor pressure to a value such that upon further isentropic expansion of the vapor it can relax to p_∞. The early time motion and the late time asymptotic position of the vapor shock has been observed by Batanov et al.[24] These authors used a neodynium glass laser ($\lambda=1.06$ μm) to vaporize a planar bismuth target in a helium background. They correlated the shock diameter $2r_{sh}$ with p_∞ (all other conditions remaining the same) and found $2r_{sh}$ to scale as $p_\infty^{-1/2}$ down to the point where $r_{sh}/2R\cong 1.5$, R being the radius of the laser spot. The spherical expansion of a steady source into an ambient gas has been studied by Simons,[25] who derived by asymptotic methods the position of the vapor shock with time. We derive below, from simple arguments, the steady-state vapor shock position and the vapor properties behind the shock.

The expansion in region 5 of Fig. 1b is adiabatic since heating of the vapor by the laser (see Appendix A) can be neglected. We have the following relations

$$p\rho^{-\gamma}=p^*\rho^{*-\gamma} \tag{9}$$

$$\rho uA=\rho^* u^* \pi R^2 \tag{10}$$

$$\rho u\frac{du}{dr}=-\frac{dp}{dr} \tag{11}$$

The star (*) indicates quantities at the sonic surface, which we take to be very near the surface of the flake. Far enough away from the flake, the flow becomes spherically symmetric and we analyze the expansion by considering that all quantities depend only on r, the distance from the center of the flake. We write that the area A is $2\pi r^2$. We integrate Eq. (11) from the surface to a point just upstream of the shock, where we assume the pressure p to be very small as compared to p^*.

§Table 2 in Ref. 23 pertaining to properties of the Knudsen layer in aluminum as a function of laser flux has incorrect values (C. Knight, private communication). We have used corrected values in plotting the aluminum vapor conditions in Fig. 4.

We find

$$u^2 = u^{*2}\frac{\gamma+1}{\gamma-1} \tag{12}$$

$$\rho = \frac{\rho^*}{2}\sqrt{\frac{\gamma-1}{\gamma+1}}\frac{R^2}{r^2} \tag{13}$$

Across the shock we have

$$p + \rho u^2 \cong p_\infty \tag{14}$$

Neglecting p as compared to ρu^2 and combining Eqs. (12-14) we calculate the positon of the shock:

$$r_{sh} = \left(\frac{\gamma}{2}\sqrt{\frac{\gamma+1}{\gamma-1}}\frac{P^*}{p_\infty}\right)^{1/2} R = 0.59\left(\frac{p_s}{p_\infty}\right)^{1/2} R \tag{15}$$

In the last step we used $\gamma = 5/3$ and replaced p^* by $0.206\,p_s$, a result derived by Anisimov[20] and confirmed by Knight[23] when the edge of the Knudsen layer corresponds to sonic conditions. The shock radius given by Eq. (17) agrees to within 7% of a result given by Simons[25] when $\gamma = 5/3$. We expect the above treatment to be valid when $r_{sh} > 2R$, i.e., when $p_s > 11 p_\infty$, and when $I_{ABS} > 3\times 10^5 \text{W/cm}^2$ ($I_{INC} > 3\times 10^6 \text{W/cm}^2$), since under these conditions u has attained at least 95% of its asymptotic value given by Eq. (12) and the p just in front of the shock is less than 1% of ρu^2.

We now relate the conditions in region 5 of Fig. 1b to the surface conditions and to the incident laser intensity. We have

$$\dot{m} = \rho^* u^* = \frac{I_{ABS}}{H_v} \tag{16}$$

$$p_s = \beta e^{-\theta_v/T_s} = 3.35\times 10^{11} e^{-35{,}500/T_s} (\text{dyne/cm}^2) \tag{17}$$

$$T^* = 0.669\,T_s \tag{18}$$

$$p^* = 0.206\,p_s \tag{19}$$

where $\theta_v = H_v/k_B$ (k_B is Boltzmann's constant). Equation (17) is the Clausius-Clapeyron relation for the saturated vapor, and Eqs. (18) and (19) are the conditions across the Knudsen layer when the flow becomes supersonic.[20] One must add to these relations the equation giving the density compression across the (strong) shock

$$\frac{\rho_5}{\rho} = \frac{\gamma+1}{\gamma-1} \tag{20}$$

Combining Eqs. (13), (15), and (18-20) we can express ρ_5 as a function of p_∞ and T_s

$$\rho_5 = \sqrt{\frac{\gamma+1}{\gamma-1}}\frac{\rho^*}{2}\frac{R^2}{r_{sh}^2} = \frac{m_A p_\infty}{0.669\gamma k_B T_s} \tag{21}$$

where m_A is the mass of the vapor atoms. From Eqs. (16-19) we can relate T_s to the absorbed flux I_{ABS}

$$T_s = \frac{\theta_v}{\ell n\left[\dfrac{0.206\beta H_v}{\alpha I_{INC}}\left(\dfrac{m_A\gamma}{0.669 k_B T_s}\right)^{1/2}\right]} = -\frac{\theta_v}{\ell n\left(BI_{INC}T_s^{1/2}\right)} \tag{22}$$

where for Al with $\alpha \cong 0.1$, $B = 1.5\times 10^{-13}(\text{W}^{-1}\cdot\text{cm}^2\cdot\text{K}^{-1/2})$.

The vapor density behind the shock is, therefore,

$$n_5 = \frac{p_\infty}{0.669\gamma k_B T_s} = -1.85\times 10^{17} p_\infty \ell n\left(BI_{INC}T_s^{1/2}\right)(\text{cm}^{-3}) \tag{23}$$

where p_∞ is expressed in atmospheres.

Equation (22) determines T_s as a function of the incident laser flux, from which one can derive the vapor density in region 5 by use of Eq. (23). This will enable us to calculate the vapor breakdown time in the following section once the initial density of the electrons is known.

III. Laser-Induced Breakdown in the Vapor

We assume that the vapor that leaves the vaporizing surface is initially in Saha equilibrium. This determines the initial electron concentration in the Knudsen layer. Due to the presence of the laser field and to the long time scale for electron-ion recombination, the electrons are uncoupled from the vapor atoms. We saw that the vapor cools as it expands through the Knudsen layer. The electron concentration remains frozen, however. Electrons are heated by inverse bremsstrahlung absorption of the radiation over a time scale of a few electron-neutral collisions. There are too few electrons initially to absorb a significant fraction of the incident flux so that the electric field the gas sees is the sum of the unattenuated incident and reflected fields. There will be an interference between these fields such that $I \cong 0$ at the surface and $I \cong 4I_{INC}$ a distance $\lambda/4$ ($=2.5\ \mu$m) away from the surface. Electron diffusion is sufficiently rapid, however, that the electrons will see an average field. One calculates, for example, that, under the conditions $p = 10$ atm, $T = 3000$ K, the free-electron diffusion distance after 10^{-10} s is 4 μm. Since, as we shall see later, the excitation and ionization times are comparable or longer than this time, it is a good approximation to consider that the electrons see the average intensity

$$I = I_{INC} + I_{REF} \cong 2I_{INC}$$

Initial Electron Concentration for Breakdown Calculations

The initial electron concentration is derived by using the Saha equation at surface conditions p_s and T_s. We have:

$$\frac{n_{es}^2}{n_s} = \left(\frac{2\pi k_B m_e T_s}{h^2}\right)^{3/2}\frac{2g^+}{g_0}\exp -(\epsilon_I/k_B T_s)$$

$$= 8\times 10^{14} T_s^{3/2}\exp\left(-\frac{69{,}400}{T_s}\right)\left(\text{cm}^{-3}\right) \tag{24}$$

where ϵ_I ($=5.98$ eV) is the ionization energy. In the last step we used $g^+ = 1$ and $g_0 = 6$ as the degeneracies of the aluminum ion and aluminum atom ground states, and expressed T_s in K.

One-Dimensional Vapor Expansion

Using reference conditions as we did in Sec. II [Eqs. (4-7)] for the scaling with i and the Clausius-Clapeyron relation for saturated aluminum vapor, we find

$$\tilde{n}_{es} = \tilde{n}_s^{1/2}\tilde{T}_s^{3/4}\exp\left[-\frac{\epsilon_I}{2K_B}\left(\frac{1}{T_s}-\frac{1}{T_{sc}}\right)\right]$$

$$= i^{0.56}\exp\left[-\frac{\epsilon_I}{2H_v}\left(\frac{H_v}{k_B T_s}-\frac{H_v}{k_B T_{s0}}\right)\right]$$

$$= i^{0.56}(\tilde{p}_s)^{\epsilon_I/2H_v} = i^{1.74} \tag{25}$$

The electron concentration upon expansion through the Knudsen layer is frozen so that

$$\tilde{n}_e = \tilde{n}_{es}(\tilde{p}/\tilde{p}_s) = i^{1.74} i^{-0.23} = i^{1.51} \tag{26}$$

Three-Dimensional Vapor Expansion

We write Eq. (24) as follows:

$$n_{es} = \left(\frac{8\times 10^{14} T_s^{1/2}}{k_B}\right)^{1/2} \beta^{1/2} e^{-(\theta_v+\theta_I)/2T_s}$$

where we used in the last step Eq. (17) and defined $\theta_I = \epsilon_I/k_B$ (= 69,400 K). The electron density in region 5 of Fig. 1b, with frozen chemistry, is given by

$$n_{e5} = n_{es}\frac{n_5}{n_s} = n_{es}\frac{p_\infty}{0.669\gamma p_s}$$

$$= \left(\frac{8\times 10^{14} T_s^{1/2}}{k_B}\right)^{1/2} \frac{\beta^{-1/2} p_\infty}{0.669\gamma} e^{-(\theta_I-\theta_v)/2T_s}$$

We can express the above as a function of $I_{\rm INC}$, by use of Eq. (22), since

$$\exp -(\theta_I-\theta_v)/2T_s = \exp -\left(\frac{\theta_I-\theta_v}{2\theta_v}\,\frac{\theta_v}{T_s}\right)$$

$$= (BI_{\rm INC} T_s)^{(\theta_I-\theta_v)/2\theta_v}$$

Table 2 Vapor properties at $I_{\rm INC} = 10^6$ W/cm^2 ($\rho/\rho_s = 0.44$, $M = 0.65$)

	Region 1	Region 2 (1-D)	Region 5 (3-D)
P, atm	32	11	1
T, K	3900	3000	4200
n, cm^{-3}	6×10^{19}	2.65×10^{19}	1.74×10^{18}
n_e, cm^{-3}	1.47×10^{16}	6.5×10^{15}	3.2×10^{14}

Application to aluminum yields ($I_{\rm INC}$ in W/cm^2, T_s in K, p_∞ in atmospheres)

$$n_{e5} = 2.8\times 10^9 (I_{\rm INC})^{0.48} (T_s)^{0.49} p_\infty \,({\rm cm}^{-3}) \tag{27}$$

Boltzmann Code Calculations of Electron Distribution Function

We have used a Boltzmann code that was written by Morgan at Joint Institute for Laboratory Astrophysics to study laser-induced breakdown in aluminum vapor. This code allows for electron-electron collisions as well as for superelastic collisions with excited states. We considered four excited states of Al as shown in Table 2, and used the cross sections described in Appendix B. The cross sections for momentum transfer σ_m, for excitation of electronic states $\sigma_{\rm exc}$, and for ionization σ_i are plotted in Fig. 5. We have lumped states 3 and 4 into one state for our calculations since the energy separation between these states is so small. The code gives the rates R_j for excitation of various excited states j of aluminum that we have considered. Calculations at different times were performed by updating the concentrations of excited states as follows

$$n_j(t+\Delta t) = n_j(t) + R_j \Delta t, \qquad j = 1,3$$

The time interval Δt between calculations was chosen such that the maximum fractional increase in n_j was less than some number (typically 0.2). We present in Figs. 6 and 7 results at $I_{\rm INC} = 10^7$ W/cm^2 and $\alpha = 0.1$. The intensity in the vapor for the calculations was taken to be $2I_{\rm INC}$. Under such conditions only 5% of the energy absorbed by the electrons went into heating the gas, the other 95% being used up in excitation of electronic states of Al. Figure 6 shows the evolution of the electron distribution function at different times. Note that the distribution functions are nearly Maxwellian up to an energy $\epsilon = 3.14$ eV, where the first inelastic process occurs (the population of excited states leading to lower excitation energies is negligible initially). The relative concentrations of the various states are shown in Fig. 7. The population of the first excited state at 3.14 eV is seen to be more than 10 times greater than that of the other states, which corresponds to the fact that most of the energy absorbed by the electrons goes into exciting the ^{2}S state of Al. At times greater than 10^{-9} s, the population of this state is large enough that superelastic collisions start to affect the electron distribution function beyond 3.14 eV. We were unable to continue the com-

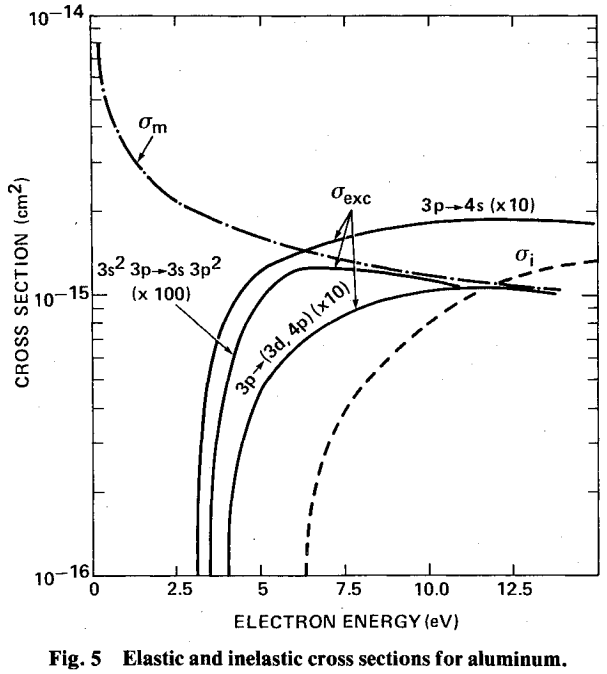

Fig. 5 Elastic and inelastic cross sections for aluminum.

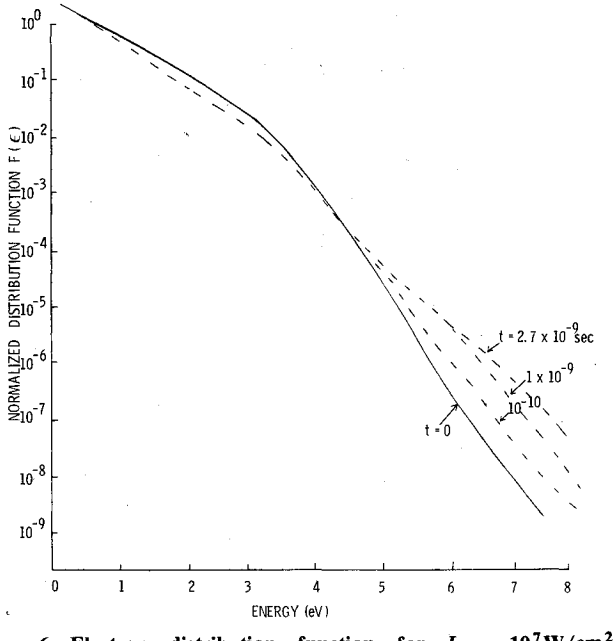

Fig. 6 Electron distribution function for $I_{\rm INC} = 10^7$ W/cm^2 ($n = 2.7\times 10^{19}$ cm^{-3}, $n_e = 6\times 10^{15}$ cm^{-3}, and $T = 3000$ K).

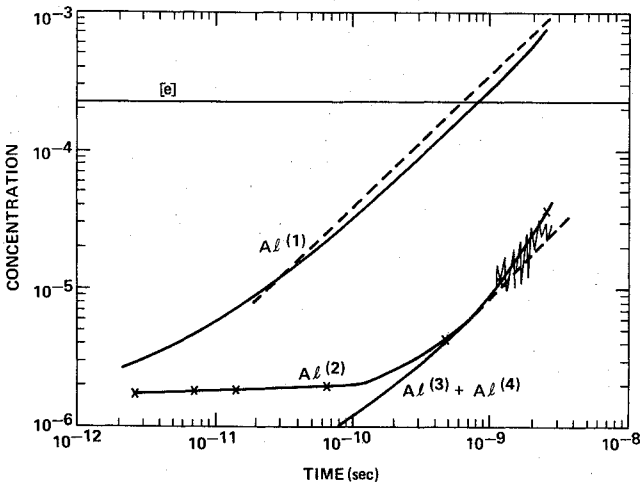

Fig. 7 Variation of excited-state populations vs time, conditions as in Fig. 6 (--- integration of Eq. (34) for n_1).

putations beyond $t = 3 \times 10^{-9}$ s due to numerical instabilities which would make the population of the highest excited state considered at 4.05 eV start fluctuating around some average value (see Fig. 7).

We have made other calculations corresponding to varying laser flux. The higher the flux the more electron-electron collisions are important, which tend to raise the distribution function at high energies. The average electron energy is in the range of 0.6-0.8 eV. At higher electron densities (higher fluxes), the average electron energy *drops*. The drop is due to the rapid population of the tail of the distribution function by electron-electron collisions resulting in higher excitation rates, but the rate of excitation is governed by energy balance considerations so the average energy must be lower. Most of the energy absorbed by the electrons goes into exciting the first excited state of aluminum so that it is a good approximation to write,

$$\frac{dn_1}{dt} = \frac{2\chi I_{INC}}{\epsilon_1} \tag{28}$$

where the factor 2 allows for the fact that the intensity is double the incident intensity and χ is the absorption coefficient to the laser radiation[26]

$$\chi = \frac{4\pi e^2 \nu n_e}{m_e(\nu^2 + \omega^2)} \tag{29}$$

where e is the electron charge, m_e the electron mass, c the speed of light, ν the elastic collision frequency of electrons with neutral atoms, and ω the laser angular frequency.

Analytical Model for Computing Breakdown Times

The results of the Boltzmann code show that initially practically all of the energy absorbed by the electrons goes into populating the first excited state of aluminum. Since the energy required to ionize from the first excited state is 5.98 − 3.14 = 2.84 eV, i.e., somewhat less than the energy required to excite the state in the first place, one expects that, at some critical population of first excited state, ionization will become more probable than excitation. For the simple model presented below, we neglect the population of the higher excited states of Al. These states will, of course, become populated at a rapid rate by impact excitation from the first excited state once the population of that state has grown sufficiently. We write the rate equations as follows:

$$\frac{dn_1}{dt} = \alpha_1 n_e n \tag{30}$$

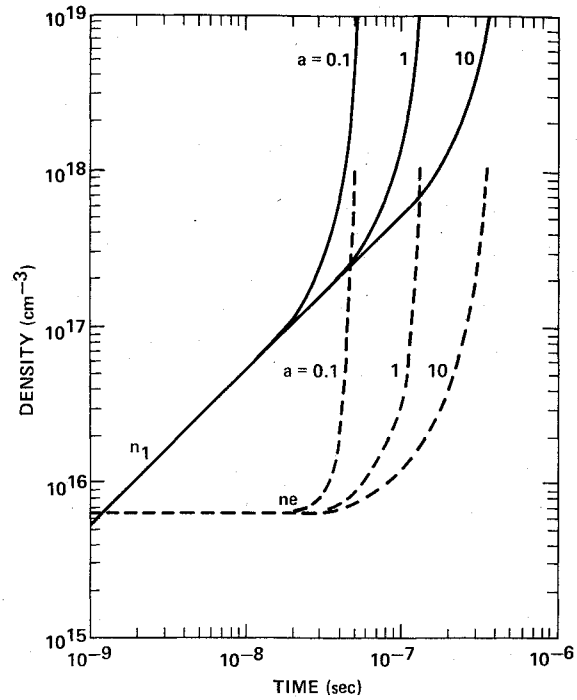

Fig. 8 Breakdown in Al vapor at $I_{INC} = 10^7$ W/cm² (initial conditions are those of Fig. 6).

$$\frac{dn_e}{dt} = \alpha_I n_e n_1 \tag{31}$$

$$2\bar{\chi} n_e n I_{INC} = \epsilon_1 \frac{dn_1}{dt} + (\epsilon + \epsilon_I)\frac{dn_e}{dt} \tag{32}$$

where $\bar{\chi}$ $(= \chi/n_e n)$ is the absorption coefficient per unit electron and atom density. The rate coefficients α_1 and α_I depend on the electron distribution function or equivalently on the average electron energy. We will neglect in the treatment that follows the electron energy ϵ, appearing in the last term of Eq. (32), as compared to ϵ_I since $\epsilon/\epsilon_I \cong 0.1$. As time goes on the state 1 becomes populated, the electron energy ϵ may vary, leading to changes in α_1 and α_I but we make the reasonable assumption that the ratio $a = \alpha_1/\alpha_I$ remains constant since the threshold energies for both processes are nearly the same and the shapes of the excitation and ionization cross-section curves vs energy are very similar. Taking the ratio of Eqs. (30) and (31) we find

$$\frac{dn_1}{dn_e} = a\frac{n}{n_1} \tag{33}$$

We integrate Eq. (33) with the initial conditions $n_1 = 0$ and $n_e = n_{e0}$ and obtain

$$n_1^2 = 2a(n_e - n_{e0})n \tag{34}$$

Inserting this value into Eq. (32) we get

$$\frac{dn_1}{dt} = \frac{2\bar{\chi} n\left(\frac{n_1^2}{2an} + n_{e0}\right) I_{INC}}{\epsilon_1 + \frac{n_1 \epsilon_I}{an}} \tag{35}$$

Integrating over time, we find

$$t = \frac{\epsilon_1}{2\bar{\chi} n I_{INC}} \left\{ \ell n \left[g\left(\frac{n_1}{n_{e0}}\right)^2 + 1 \right] + g^{-1/2} \tan^{-1}\left(g^{1/2}\frac{n_1}{n_{e0}}\right) \right\} \tag{36}$$

with $g = n_{e0}/(2an)$.

The solution to Eqs. (34) and (36) is straightforward since t and n_e are functions of n_1 only. We have plotted in Fig. 8 the solution for $I_{INC}=10^7 W/cm^2$ and three values of a (namely 0.1, 1, and 10). This figure shows the general features of the breakdown: there is a lag time when n_e remains constant and n_1 increases linearly with time. The rate of increase in n_1 is easily derived from Eq. (32) by setting $dn_e/dt=0$, and also from Eq. (36) by noting that $g \ll 1$ and that the second term on the right-hand side is the dominant term

$$n_1 = 2\bar{\chi} n_e n I_{INC} t/\epsilon_1 \tag{37}$$

The electron density starts increasing when the excited-state density has reached a value such that, in Eq. (35), the first term in the numerator dominates. This occurs when $n_1 > n_{1c}$, where n_{1c} is given by

$$n_{1c} = (2ann_{e0})^{1/2} \tag{38}$$

This occurs at a time [combining Eqs. (37) and (38)]

$$t_c = \frac{n_{1c}\epsilon_1}{2\bar{\chi} n_{e0} n I_{INC}} = \left(\frac{a}{2n_{e0}n}\right)^{1/2} \frac{\epsilon_1}{\bar{\chi} I_{INC}} \tag{39}$$

t_c is seen to scale as $a^{1/2}$. The actual value of a, as obtained from the cross-section formula of Appendix B, is expected to be near unity.

The treatment given above has not taken into account superelastic collisions which would result in the deactivation of the excited state with the energy landing in the electrons. Detailed balancing gives us the excited-state density at which energy gained from superelastic collisions with the excited-state population balances energy lost by inelastic collisions with ground-state atoms:

$$\hat{n}_1 = n \frac{g_1}{g_0} \exp - \frac{\epsilon_1}{\langle \epsilon \rangle} \tag{40}$$

where $\langle \epsilon \rangle$ is the average electron energy. Setting $\epsilon_1 = 3.14$ eV, $\langle \epsilon \rangle = 0.7$ eV, $g_1 = 2$, $g_0 = 6$, $n = 2.6 \times 10^{19} cm^{-3}$, we find $\hat{n}_1 = 10^{17} cm^{-3}$. When n_1 approaches this value the average electron energy (which had remained constant) starts rising so that Eq. (40) is almost satisfied. The linear growth rate of n_1 given by Eq. (34) still holds, however, since the energy involved in heating the electrons is small as compared to the energy involved in exciting the vapor atoms. Superelastic collisions may, however, decrease the breakdown time somewhat, since some electrons will have gained enough energy for direct impact ionization of the ground-state atoms.

IV. I vs t Map for Initiation of Breakdown over Aluminum Surfaces

We are now in a position to map on an intensity vs time graph the various regimes for initiation of breakdown over aluminum surfaces at 10.6 μm. For definiteness we consider the breakdown initiated by a surface defect which is a flake of thickness $\delta = 0.2$ μm and of transverse radius $R = 6$ μm. These are reasonable values for the larger flakes,[27] as inferred from electron micrograph pictures of the surface and analysis of the breakdown data.[7,8] Scaling of our results to other values of R and δ are straightforward. The map is shown in Fig. 9.

We have plotted the time for the flake to reach the vaporization temperature given by Eq. (3) with an average value of $1/\alpha = 20$ ($\alpha = 5\%$). This line has a slope of -1 (the abscissa of this curve scales as δ), and corresponds to a constant absorbed fluence of 2 J/cm^2. For incident intensities $> 3 \times 10^9 W/cm^2$, the flake does not heat up uniformly and one must treat the flake as a semi-infinite heat conductor, which gives a line of slope $-\frac{1}{2}$. For $I > 3 \times 10^9 W/cm^2$, bulk vaporization will occur simultaneously with flake vaporization. One must note, however, that at fluxes of

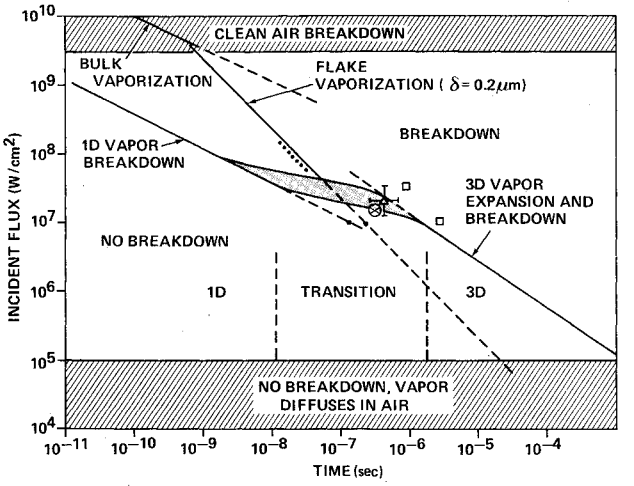

Fig. 9 I vs t for vapor breakdown over Al surfaces at $\lambda = 10.6$ μm. This map is for flake parameters $\delta = 0.2$ μm and $R = 6$ μm; dotted-line segment represents our analysis of data of Ref. 9, □ breakdown results on Mg targets of Ref. 28 which have been scaled (Ref. 8) to equivalent conditions on Al targets, ⊗ Ref. 29, and △ Ref. 30.

$> 3 \times 10^9 W/cm^2$ one is above the threshold for breakdown of clean air[9-11] and it is doubtful whether the laser beam will reach the target.

We have next plotted in Fig. 9 the one-dimensional vapor breakdown time. This time is shorter than the flake vaporization time for fluxes $I_{INC} > 10^7 W/cm^2$ so that the time lag to heat the flake dominates the plasma initiation time. The slope of the line is -2.15 and is obtained from Eq. (39) with the use of Eqs. (6), (7), and (26).

$$\tau_{VBr} \propto \frac{1}{(n_{e0}n)^{1/2}} \frac{1}{I_{INC}} \propto i^{-2.15}$$

We then draw in Fig. 9 the vapor breakdown curve in the three-dimensional expansion regime, occurring at fluxes $I_{INC} < 10^7 W/cm^2$. This line has a slope -1.24 and corresponds to times longer than the flake heating to vaporization time. This line is obtained by calculating the vapor breakdown time in the shocked vapor where, from Eq. (37), n_{e5} scales as $i^{0.48}$ and n_5 has a negligible dependence on I_{INC} [see Eq. (23)]. Equation (38) then gives:

$$\tau_{VBr} \propto \frac{1}{(n_{e0}n)^{1/2}} \frac{1}{I_{INC}} \propto \frac{1}{(i^{0.48})^{1/2}} \frac{1}{i} = i^{-1.24}$$

Between the 10^7 and 10^8 W/cm^2 incident on the target is a region where neither one- nor three-dimensional breakdown times hold and we have joined the curves with artistic liberty.

We have also drawn in Fig. 9 some of the measured plasma initiation times.[8,28-30] The breakdown times measured by Walters et al.[7,8] occurred during the rising portion of the gain-switched spike. We have represented the range of data in Fig. 9 by a dashed-line segment corresponding to an equivalent square pulse having the same constant fluence (1.7 J/cm^2) that they found was required for plasma initiation and having the intensity that was measured at the time of breakdown. One should note that the range of intensities at the time of breakdown is a factor of three smaller than the range of *peak* spike intensities that they used to plot their data. The measured initiation times shown in Fig. 9 fall near or inside the theoretically computed breakdown zone. The agreement is found to be satisfactory. More data points are required in the flux regime 10^7-10^8 W/cm^2 in order to substantiate the plasma-initiation model developed in this paper more fully.

V. Discussion and Conclusions

We have shown in the previous section that a model which includes the following events: 1) rapid evaporation of thermally insulated "flakes" followed by 2) laser-induced breakdown in the metal vapor with a one-dimensional (early time) or three-dimensional (late time) expansion of the vapor, could explain the (limited) data on laser-induced breakdown of aluminum surfaces.

This model is in agreement with and provides a physical basis for the empirical correlation of data made by Musal[3] whereby prompt breakdown over aluminum surfaces is associated with an intensity of $\sim 1 J/cm^2$ delivered at an intensity exceeding $10^7 W/cm^2$. CO_2 laser pulse profiles are usually characterized by an initial gain-switched spike having a peak intensity 2-10 times the intensity averaged over the whole pulse. The full width at half maximum (FWHM) spike width is in the 50-200 ns range. When the peak intensity in the spike exceeds $3\times 10^7 W/cm^2$, we would expect from Fig. 9 that the breakdown would occur within the spike. The agreement with the data of Walters[7,8] at fluxes larger than $3\times 10^7 W/cm^2$ is to be expected since the breakdown is determined by the time it takes the flake to vaporize. This time varies with the flake thickness δ and we use almost the same δ ($=0.2$ vs 0.3 μm) that Walters et al.[7,8] used to explain their data. One would expect a surface to have a whole range of defect sizes. The fact that shorter breakdown times are not observed with flakes of smaller thicknesses may be due to rapid mixing of vapor with the air and the small lateral extent of the defect leading to three-dimensional geometry immediately upon vaporization.

An important result of this study is that the rapid breakdown in the metal vapor is not due to the occurrence of an immediate avalanche (which would occur in the absence of inelastic processes excepting ionization) as has been erroneously suggested elsewhere,[28] but due to ionization from excited states which are populated by inelastic collisions with electrons. Starting from a Saha equilibrium at the metal surface, we have found by using a Boltzmann code that the delay time for populating the first excited state of Al to a point where electron impact ionization of this state leads to avalanche breakdown is very short. It is not obvious, however, that our choice of Saha equilibrium of the vapor as it leaves the surface is the proper one since vaporization will occur through a Mott transition.[31] The metal properties at the Mott transition (under an applied I_{INC}) should be the ones which determine in effect the initial electron concentration.

In this paper we have not considered radiative losses. Bremsstrahlung losses should become important only when the breakdown has occurred. Radiative de-excitation of the first excited state can be neglected over time scales less than 10^{-8} s. Furthermore, the line radiation should be trapped and a rough estimate of energy losses assuming black-body radiation within the line show these losses to be negligible (for $T_e=0.6$ eV) as compared to the inverse bremsstrahlung heating of the electrons in the vapor. Motion of the flake due to the vapor-induced back pressure has been considered and has been found to be negligible over the time scale of interest ($t<10^{-5}$ s).

Also, we have not considered in this paper heat conduction losses along the flake into the bulk metal. The ratio of absorbed fluence to lateral conduction losses scales as $\alpha I_{INC} R^2/\delta$ and, for the flake parameters considered in this paper ($R=6$ μm, $\delta=0.2$ μm), heat conduction losses become significant when I_{INC} is below $5\times 10^5 W/cm^2$. The breakdown treatment in Sec. IV neglected elastic losses to the neutrals. At fluxes below $3\times 10^5 W/cm^2$ these become important and the quasiequilibrium gas breakdown model used by Thomas[32] to study initiation of laser-supported conduction waves becomes appropriate.

Although we have considered only one metal (Al) at one wavelength (10.6 μm) the treatment here can be easily extended to other metals and wavelengths. One requires, however, a knowledge of absorptivity vs wavelength and temperature. The presence and size of defects should depend both on the mechanical properties of the metal and on the method of preparation of the surface. Breakdown thresholds should depend on the ratio of the vaporization temperature to the ionization energy, which determines the initial electron concentration. Excitation of the first excited state should play an equally important role, although this state in general would not be half way between the ground state and the ionization continuum. The treatment in Sec. IV where we assumed a constant a would have to be modified accordingly.

Appendix A: Heating of the Vapor during Breakdown

We estimate the vapor heating during the lag time before breakdown. We will show that for all practical purposes heating of the vapor can be neglected. Two mechanisms for heating of the vapor are possible:

1) Collisional deactivation of excited states of Al: $Al + Al^* \rightarrow 2Al$.

2) Electron-neutral elastic collisions:
$e(\epsilon+\Delta\epsilon) + Al(\epsilon') \rightarrow e(\epsilon) + Al(\epsilon'+\Delta\epsilon)$.

The first reaction is highly improbable because of the large energy mismatch ($\Delta\epsilon > 3$ eV). The second reaction, following the results of the Boltzmann code calculations, causes a (small) fraction η of the absorbed laser energy to go into heating of the gas.

We saw in Sec. III that breakdown occurs very rapidly once the first excited-state density has reached the critical value $n_{1c} = (2ann_{e0})^{1/2}$. The energy dumped into heating of the gas during the lag time t_c is therefore $\eta n_{1c}\epsilon_1$, which corresponds to a relative temperature rise (or relative energy rise per neutral atom)

$$\frac{\Delta T}{T} = \frac{\Delta\epsilon}{\epsilon} = \frac{\eta\epsilon_1 n_{1c}}{nkT} = \frac{\eta\epsilon_1}{kT}\left(\frac{2an_{e0}}{n}\right)^{1/2}$$

As a numerical example, consider the case $I_{INC}=10^7 W/cm^2$, for which $\eta=0.05$, $\epsilon_1=3$ eV, $kT=0.3$ eV, $n_{e0}=6\times 10^{15} cm^{-3}$, $n=2\times 10^{19} cm^{-3}$, and $a=1$. We find $\Delta T/T=1\%$ or $\Delta T=30$ K.

Appendix B: Cross Sections for Aluminum

The electron-aluminum atom momentum transfer cross section has been calculated by Hyman et al.[33] based on a model for collisions with polarizable atoms. The cross section is

$$\sigma_m = \frac{3.58\times 10^{-15}}{\sqrt{\epsilon}} (cm^2) \qquad (B1)$$

where ϵ is expressed in eV. The collision frequency is, therefore, independent of electron energy (or temperature) since

$$\nu = n\langle\sigma_m u_e\rangle = 2.12\times 10^{-7} n \ (s^{-1}) \qquad (B2)$$

The excitation cross section is given by[34]

$$\sigma_{ij} = 6.9\times 10^{-18}\frac{f_{ij}}{\epsilon\epsilon_{ij}} b(\epsilon/\epsilon_{ij}) (cm^2) \qquad (B3)$$

where f_{ij} is the f number for the transition $i\rightarrow j$, ϵ_{ij} the threshold energy (eV) for the excitation, and $g(\epsilon/\epsilon_{ij})$ a tabulated function[34] which is 0 for $\epsilon<\epsilon_{ij}$ and peaks at $\epsilon/\epsilon_{ij}=3$. f_{ij} and ϵ_{ij} are presented in Table B1. Note that the transitions to state 2 are optically forbidden because there is a spin flip. For transitions involving this state and other optically forbidden transitions, we have arbitrarily chosen a small f number (0.01) in Eq. (B3) for electron impact-induced transitions since these are *not* forbidden.

The ionization cross section is given by

$$\sigma_{jI} = \frac{1.63\times 10^{-14}\eta}{\epsilon_{jI}\epsilon} F\left(\frac{\epsilon}{\epsilon_{jI}}\right) (cm^2) \qquad (B4)$$

Table B1 ϵ_{ij} (eV) and ν_{ij} for transitions in aluminum

State i / j	0 $3s^2 3p$ $^2P^0$	1 $3s^2 4s$ ^2S	2 $3s3p^2$ ^4P	3 $3s^2 3d$ ^2D	4 $3s^2 4p$ $^2P^0$
0	ϵ_{ij} =	3.14	3.6	4.02	4.1
	f_{ij} =	0.115	x[a]	0.175	x
1	ϵ_{ij} =		0.46	0.84	0.9
	f_{ij} =		x	x	1.41
2	ϵ_{ij} =			0.42	0.5
	f_{ij} =			x	x
3	ϵ_{ij} =				0.08
	f_{ij} =				(1)[a]

[a] x = forbidden transiton: ( ) = estimated f number.

where η is the number of optical electrons, ϵ_{jI} ($=\epsilon_I - \epsilon_j$) is the binding energy (eV) of the excited state j, and F is a tabulated function.[34] The cross sections with ground-state atoms that we have derived from these formulas and used are plotted in Fig. 5.

References

[1] Raizer, Y. P., "Heating of a Gas by a Powerful Laser Pulse," *Soviet Physics, JETP Letters,* Vol. 21, Nov. 1965, pp. 1009-1017.

[2] Raizer, Y. P., "The Feasibility of an Optical Plasmatron and Its Power Requirements," *Soviet Physics, JETP Letters,* Vol. 11, May 1970, pp. 302-305.

[3] Boni, A., Su, F., Thomas, P., and Musal, H., "Theoretical Studies of Laser-Target Interactions," Science Applications Inc., Midterm Tech. Rept. SAI 76-722LJ, Aug. 1976.

[4] Thomas, P. D. and Musal, H. M., "A Theoretical Study of Laser Target Interaction," Lockheed Palo Alto Research Center, Final Tech. Rept. LMSC D-352890, Contract DAAH01-72-C-0930, Aug. 1973.

[5] Thomas, P. D. and Musal, H. M., "A Theoretical Study of Laser Target Interaction," Lockheed Palo Alto Research Laboratory, First Semi-Annual Tech. Rept. LMSC D-313142, 1972.

[6] Steverding, B., "Ignition of Laser Detonation Waves," *Journal of Applied Physics,* Vol. 45, Aug. 1974, pp. 3507-3511.

[7] Walters, C. T., Barnes, R. H., and Beverly, R. E., "An Investigation of Mechanisms of Initiation of Laser-Supported Absorption (LSA) Waves," Battelle Columbus Laboratories, Final Report for Period April 1973 - Aug. 1975, ARPA Order 2113.

[8] Walters, C. T., Barnes, R. H., and Beverly, R. E., III, "Initiation of Laser Supported Detonation (LSD) Waves," *Journal of Applied Physics,* Vol. 49, May 1978, pp. 2937-2949.

[9] Smith, D. and Brown, R., "Aerosol Induced Air Breakdown with CO_2 Laser Radiation," *Journal of Applied Physics,* Vol. 46, March 1975, pp. 1146-1154.

[10] Canavan, G., Proctor, W., Nielsen, P., and Rockwood, S., *IEEE Journal of Quantum Electronics,* Vol. QE8, 1972, pp. 564-565.

[11] Weyl, G., "Ionization Path Formation in Gases Using a Laser with Retractable Focus," *Journal of Physics, D: Applied Physics,* Vol. 12, Jan. 1979, pp. 33-49.

[12] Edwards, A., Ferriter, N., Fleck, J. Jr., and Winslow, A., "A Theoretical Description of the Interaction of a Pulsed Laser and a Target in an Air Environment," Lawrence Livermore National Laboratories Rept. UCRL-51489, Nov. 1973.

[13] Nielson, P. E., "Metal Vapor Breakdown in Quantum Kinetic and Temperature Models," Air Force Weapons Laboratory Rept. AFWL-TR-73-131, June 1973.

[14] Reilly, D. and Rostler, P., "Prebreakdown Target Vaporization and Enhanced Thermal Coupling," Avco Everett Research Laboratory, Final Tech. Rept., Contract N00014-73-C-0457, Aug. 1974.

[15] Born, M. and Wolf, E., *Principles of Optics* (3rd Ed.), Pergamon Press, New York, 1965, p. 624.

[16] Beattie, J., "The Anomalous Skin Effect and the Infrared Properties of Silver and Aluminum," *Physica,* Vol. 13, 1957, pp. 898-902.

[17] Bennett, H., Silver, M., and Ashley, E., "Infrared Reflectance of Aluminum Evaporated in Ultra High Vacuum," *Journal of the Optical Society of America,* Vol. 53, Sept. 1963, pp. 1089-1095.

[18] Roll, A. and Motz, Z., "Der Elektrische Widerstand von Metallischen Schmelzen," *Zeitschrift fur Metallkunde,* Vol. 48, May 1957, pp. 272-280.

[19] Ujihara, K., "Reflectivity of Metals at High Temperatures," *Journal of Applied Physics,* Vol. 43, May 1972, pp. 2376-2382.

[20] Anisimov, S., "Vaporization of Metal Absorbing Laser Radiation," *Soviet Physics, JETP,* Vol. 27, July 1968, pp. 182-183.

[21] Thomas, P. D., "Estimates of the Early-Time Gas Dynamics of Laser Beam-Target Interaction," Lockheed Palo Alto Research Laboratory Rept. LMSC-D-267440, June 1977.

[22] Pirri, A., "Analytic Solution for Laser-Supported Combustion Wave Ignition Above Surfaces," AIAA Paper 76-23, Washington, D. C., 1976.

[23] Knight, C., "Theoretical Modeling of Rapid Surface Vaporization with Backpressure," *AIAA Journal,* Vol. 17, May 1974, pp. 519-523.

[24] Batanov, V., Bunkin, F., Prokhorov, A., and Fedorov, V., "Immobile Shock Upon Stationary Evaporation of Metal by Laser Radiation," *Soviet Physics, JETP Letters,* Vol. 11, Jan. 1970, pp. 69-72.

[25] Simons, G., "The Large Time Behavior of a Steady Spherical Source Expanding Into an Arbitrary Ambient Gas," AIAA Paper 70-232, Jan. 1970.

[26] Zel'dovich, Y. and Raizer, Y., *Physics of Shock Waves and High Temperature Hydrodynamic Phenomena,* Vol. I, Academic Press, New York, 1966, p. 283.

[27] Walters, C., private communication. Battelle Memorial Institute, Columbus, Ohio, 1980.

[28] Barshukov, A., Bunkin, F., Konov, V., and Lyubin, A., "Investigation of Low Threshold Gas Breakdown near Solid Targets by CO_2 Laser Radiation," *Soviet Physics JETP,* Vol. 39, Sept. 1974, pp. 469-477.

[29] Maher, W., Hall, R., and Johnson, R., "Experimental Study of Ignition and Propagation of Laser-Supported Detonation Waves," *Journal of Applied Physics,* Vol. 45, May 1974, pp. 2138-2145.

[30] McKay, J. and Schriempf, J., "Anomalous Infrared Absorptance of Aluminum under Pulsed 10.6 μm Laser Irradiation in Vacuum," *Applied Physics Letters,* Vol. 55, Sept. 1979, pp. 433-434.

[31] Mott, N. F., *Metal-Insulator Transitions,* Taylor and Francis, London, 1974.

[32] Thomas, P. D., "Laser Absorption Wave Formation," *AIAA Journal,* Vol. 13, Oct. 1975, pp. 1279-1286.

[33] Hyman, H. A., Kivel, B., and Bethe, H., "Inverse Neutral Bremsstrahlung for Highly Polarizable Systems," AVCO Everett Research Laboratory, AMP 333, April 1973.

[34] Allen, C. W., *Astrophysical Quantities* (2nd Ed.), Athlone Press, London, 1963, p. 42.